Korean J. Chem. Eng., 36(6), 988-995 (2019)
DOI: 10.1007/s11814-019-0270-6

pISSN: 0256-1115
eISSN: 1975-7220

One-pot synthesis of highly stable and concentrated silver nanoparticles with enhanced catalytic activity

Fiaz Hussain[***], Samy M. Shaban[*,], Jinhwan Kim[*,†], and Dong-Hwan Kim[*,**,†]**

*School of Chemical Engineering, Sungkyunkwan University, Suwon 16419, Korea
**Biomedical Institute for Convergence at SKKU (BICS), Sungkyunkwan University, Suwon 16419, Korea
***Polymer Department, Sungkyunkwan University, Suwon 16419, Korea
(*Received 19 January 2019 • accepted 8 April 2019*)

Abstract−Well-dispersed silver nanoparticles (AgNPs) were synthesized using a benign, one-pot process based on a low-cost wet chemistry technique. Monoethanolamine was used as a strong reducing agent and poly(acrylic acid) (PAA) was used as a stabilizing agent. After the addition of these reagents to a reaction system, one-pot synthesis of AgNPs was completed in ~45 min at 75 °C with a reaction efficiency of 92.4%. The average particle size of the aqueous dispersion of AgNPs was 14.83±5.96 nm, and the dispersion remained stable even after 14 months in an ambient dark environment, which may be due to the electrostatic repulsion of the carboxylate anions of the stabilizing agent. The role of PAA in the stabilization of the AgNPs was analyzed via Fourier transform infrared spectroscopy and energy-dispersive X-ray spectroscopy. The highly stable AgNPs in the aqueous system showed high catalytic activity for the reduction of methylene blue and *p*-nitrophenol in the presence of sodium borohydride as the reducing agent based on pseudo-first-order kinetics.

Keywords: One-pot Synthesis, Silver Nanoparticles, High Yield, Stability, Catalytic Activity, Methylene Blue, *p*-Nitrophenol

INTRODUCTION

Metallic nanoparticles have attracted attention because of their many desirable and unique properties [1,2]. Among the numerous metallic nanoparticles that have been investigated to date, silver nanoparticles (AgNPs) are well known for their wide range of applications, such as in optics [2], electronics [3,4], highly stretchable circuits, localized surface plasmon resonance (SPR) [5], sensors [6], and medicine [7], in addition to their excellent catalytic [8] and antimicrobial [9,10] properties. However, nanoparticles have a high tendency to undergo oxidation and aggregation in practical applications, which suggests a need for enhancement of their colloidal stability [11]. Researchers have been keen to develop highly concentrated and stable dispersions of AgNPs with uniform particle size because they potentially have versatile applications in the industry. However, the development of a highly stable dispersion of AgNPs is a challenge, given the importance of stabilization of nanoparticles in numerous applications [12]. Usually, the synthesis of narrow-sized AgNPs involves the thermolysis of a silver source in nonpolar and toxic solvents, which can lead to environmental issues [13,14]. The hydrophobic nature of nanoclusters limits their practical applications, especially in biological systems, in which water solubility of nanoparticles is an important requirement. Additional surface modifications are required to make the hydrophobic nanoparticles water-soluble [15,16].

In view of the increasing demand for AgNPs, many researchers have attempted to synthesize highly concentrated, stable dispersions [17,18]. AgNPs can be synthesized by various chemical, physical, and biological methods [19]. However, research on the synthesis of highly concentrated, stable colloids of AgNPs is limited. Stabilization of highly concentrated AgNPs is difficult because of their high surface energy and high surface-area-to-volume ratio. Recently, numerous studies have been conducted on the synthesis of highly concentrated, stable dispersions of AgNPs (Table 1). However, the utilization of these synthesis techniques in industrial applications is hindered by low reaction efficiency, high energy input, use of toxic and environmentally hazardous chemicals, high cost, complex reaction, large size distribution, and long reaction time [4,16,20-27].

The carboxylate groups in poly(acrylic acid) (PAA), which is inherently biocompatible, confer good surface binding properties [28] for enhanced colloidal stability of silver nanocrystals in aqueous phase [29-31]. Highly stable, low-concentration core-shell nanoparticles have been synthesized at high temperatures by a polyol process. However, this synthesis process is rather complex and requires relatively expensive reagents in addition to involving a long reaction time [32]. The synthesis of concentrated AgNPs and their conductive properties have been reported [20,21]. However, their industrial applications are limited because of their long reaction time, complex synthesis processes, and broad size distribution. Furthermore, the large size of synthesized AgNPs inhibits their use in enhanced catalytic and antibacterial applications [10,33].

In the present study, we synthesized highly concentrated, stable, and uniform colloids of AgNPs by an environmentally benign and facile wet chemistry technique. We used monoethanolamine as a reducing agent because it is relatively inexpensive and commercially

†To whom correspondence should be addressed.
E-mail: jhkim@skku.edu, dhkim1@skku.edu
‡F. H. and S. M. S. contributed equally to this work.

available and has low toxicity. PAA was used as a capping agent. The colloidal dispersion of AgNPs was stable for more than 14 months under ambient environmental conditions. The concentration of the synthesized AgNPs was ca. 83,070 ppm after washing. Our developed synthesis approach has several distinct advantages: use of relatively inexpensive starting reagents, a short reaction time, high reaction efficiency, and a high concentration of the synthesized product. Thus, the synthesis process can be characterized as being environmentally friendly, which makes it ideal for industrial applications. We also investigated the catalytic properties of the synthesized AgNPs in terms of the reduction of pollutants, such as *p*-nitrophenol and methylene blue (MB).

EXPERIMENTAL SECTION

1. Materials

Silver nitrate ($AgNO_3$, ≥99% purity), monoethanolamine (>99.5% purity), PAA (M_w: 1800), 4-nitrophenol (*p*NP), MB, and sodium borohydride ($NaBH_4$) were used as received without any further purification. These analytical-grade materials were purchased from Sigma-Aldrich. Ultra-pure deionized water prepared using a Milli-Q SP reagent water system (Millipore, Milford, MA) was used in all experiments.

2. Synthesis of Silver Nanoparticles

First, 4.1 mL of monoethanolamine, 10 mL of $AgNO_3$ (0.83 M), and 0.55 g PAA were mixed at room temperature, which yielded a nearly transparent mixture. The mixture was heated to 75 °C at 500 rpm. The nucleation process began after 10 min and the solution turned light yellow in color. As the reaction proceeded, the concentration of AgNPs increased, which resulted in color changes at different intervals (Fig. S1, supplementary file). The entire reaction was completed in approximately 45 min, after which the nanoparticle solution was cooled to room temperature. The nanoparticles capped with PAA were collected by centrifugation at 11,000 rpm for 15 min and then rinsed 5 times with water. The pH of the AgNP dispersion was 8.84.

3. Characterization

A UV-Vis spectrophotometer (JASCO V-770) was used for measurement of the characteristic absorbance peak of the AgNPs in the range of 300-900 nm, in addition to examination of the catalytic properties of the as-prepared AgNPs. The surface morphology of the particles was analyzed using a field emission scanning electron microscope (JEOL JSM-7600F) at an accelerating voltage of 15 kV and a high-resolution transmission electron microscope (JEM-3010). The particle size distribution were analyzed using image processing software (Image J bundled with 64-bit Java 1.8.0-112, available for download at https://imagej.nih.gov/ij/index.html). Elemental analysis of the AgNPs was performed using an energy-dispersive X-ray spectrometer (X-MAX 50). A high-power thin-film X-ray diffractometer system (D8 Advance) was utilized to characterize the structure of the synthesized nanoparticles. Samples for X-ray diffraction (XRD) analysis were prepared by dropping the aqueous AgNPs onto a silicon wafer and subsequently drying the wafer in an oven at 65 °C. A sample was scanned in the 2θ range of 20-80° with a scanning speed of 2θ/min. The concentration of the synthesized AgNPs in solution was determined using an inductively coupled plasma mass spectroscopy (ICP-MS) apparatus (Agilent 7500).

The synthesized nanoparticles with a PAA-modified surface were analyzed using a Fourier transform infrared (FTIR) spectrophotometer (JASCO, FT/IR-4700). The nanoparticles were washed with deionized water, and a powder sample for FTIR analysis was obtained after drying the washed nanoparticles at 65 °C. The sample was scanned in the range of 300-4,000 cm^{-1} with a scanning speed of 4 mm/min. Zeta potential analysis of the sample in water was performed using a Zetasizer Nano ZS (Malvern Instruments).

4. Catalytic Reduction Activity of AgNPs@PAA

The catalytic activity of the synthesized AgNPs@PAA was examined using a modified version of the process developed by Zeng et al. [34]. The catalytic activity was examined against *p*NP and MB using $NaBH_4$ as a reducing agent. In a typical procedure for examining the catalytic activity against MB, 2 mL of freshly prepared $NaBH_4$ aqueous solution (0.02 M) was mixed with 20 μL of MB aqueous solution (5 mM), and the final volume was increased to 3 mL in a standard quartz cell by using distilled water. Finally, 5 or 10 μL of the as-prepared AgNPs@PAA catalyst (0.152 mg/mL) was added to the mixture and UV-Vis spectroscopy was immediately performed at different time intervals in the range of 500-800 nm. To investigate the catalytic activity against *p*NP, 2 mL of deionized water was added to 1 mL of freshly prepared $NaBH_4$ (1 M) and 100 μL of *p*NP (5 mM) in a standard cuvette. To examine the catalytic reduction of *p*NP, 2 or 4 μL of the as-prepared catalyst (0.152 mg/mL) was added to the mixture, which was then scanned using the UV-Vis spectrophotometer in the range of 250-550 nm.

RESULTS AND DISCUSSION

1. Characterization of AgNPs@PAA

The wet chemical reduction method was used to convert the high concentration of $AgNO_3$ (0.83 M) into AgNPs by using PAA as a stabilizing agent to produce AgNPs@PAA. The morphology of the synthesized AgNPs@PAA was investigated by FE-SEM and high-resolution transmission electron microscopy (HR-TEM), and the results are shown in Figs. 1(a) and 1(b), respectively. Fig. 1(a) demonstrates the uniform and spherical morphology of the as-prepared AgNPs@PAA, which was confirmed by HR-TEM (Fig. 1(b)). The SEM image was analyzed using the Image J image processing software to determine the size distribution; the analysis results indicated that the particles had a narrow size distribution with an average size of 14.83±5.96 nm, as depicted in Fig. 1(c). The Zeta potential of the synthesized AgNPs@PAA was determined to be −21±1.3 mV. This is also indicative of their high aqueous stability. The concentration of the acquired AgNPs@PAA was determined by ICP-MS to be 83,070 ppm with a synthesis yield of 92.4%; this value is listed in Table 1 along with previously reported values for comparison purposes. To the best of our knowledge, this is the first time that such a high concentration of AgNPs has been obtained. Fig. 1(d) shows the UV-Vis spectra of the as-prepared AgNPs@PAA. The UV-vis data shows a sharp absorbance band at λ=422 nm, indicating the formation of monodispersed AgNPs with a narrow size distribution. The sample was diluted 800 times before the UV-Vis measurement.

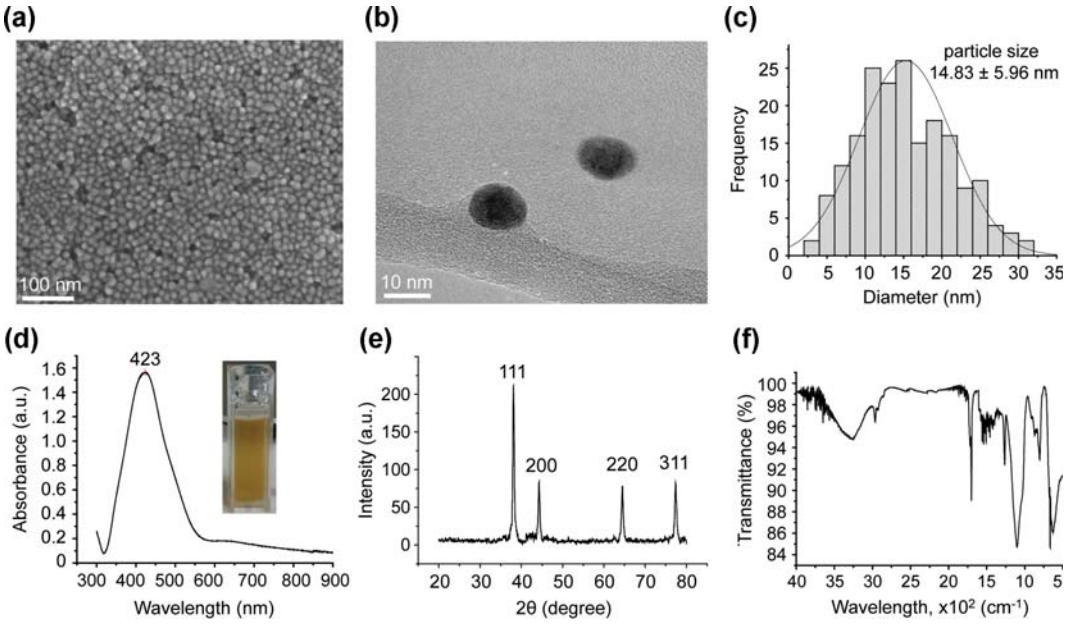

Fig. 1. (a) FE-SEM image of highly concentrated AgNPs@PAA; (b) HR-TEM image of AgNPs@PAA; (c) analysis of AgNPs@PAA size distribution calculated using Image J software; (d) UV-Vis spectra of dispersed suspension of AgNPs@PAA, where the inset shows an optical image; (e) XRD pattern of highly crystalline AgNPs@PAA; and (f) FTIR spectrum of AgNPs@PAA.

Table 1. Characteristics of AgNPs synthesized in previous studies in comparison with those synthesized in the present study

Initial $AgNO_3$ conc. (M)	Synthesis time/ stability	Drawbacks of synthesis process	AgNP size (nm)	Reaction efficiency (yield %)	Reference
1.65	2 h/3 months	Long reaction time, broad size distribution (20-230 nm), and no reproducibility	30	-	[4]
1.9	25 h/-	Long reaction time with extreme precautions	30	-	[20]
0.94	45 min/6 months	Requirement of relatively high temperature, two steps, and high pH of 9.5 to ensure stability. Broad size distribution (5-80 nm)	11	-	[21]
0.16	4.5 h/-	Two phases and a complex reaction	4	-	[22]
0.27	7 min/-	Stable only below concentration of 0.3 M	26	-	[23]
0.1	4 h/8 months	Lengthy process and low reaction efficiency	30	25	[16]
0.43	10 h	Long reaction time, high power of 200 W, and non-environmental solvents	20-30	-	[25]
0.025	6.5 h/-	Long reaction time and complex and expensive process	4	82	[26]
0.02	2 min/-	Low concentration and use of hazardous and highly toxic chemicals	10	94	[27]
0.83 M	45 min/14 months	-	14	92.4	This study

The well-crystallized structure of AgNPs detected by the XRD analysis is shown in Fig. 1(e). The four sharp peaks at 39.7, 44.3, 64.5, and 77.4° can be attributed to the (111), (200), (220), and (311) crystalline planes, respectively, of the face-centered cubic (FCC) structure of metallic silver. These distinct peaks indicate that metallic silver particles were successfully obtained. In accordance with the Joint Committee on Powder Diffraction Standards (JCPDS) database (file no. 00-004-078383), the synthesis of pure and well-crystallized AgNPs@PAA is confirmed from this XRD result.

Next, the role of PAA in the capping process of AgNPs was confirmed by FTIR spectroscopy, as shown in Fig. 1(f). The results clearly confirm that the surface of the nanoparticles was capped by PAA. The broad band at 3,270 cm^{-1} is attributed to the -OH stretching of the carboxylic group, and the sharp absorbance bands at 2,964 and 2,823 cm^{-1} can be assigned to CH- asymmetric and symmetric stretching, respectively, occurring in PAA. The strong signal at 1,700 cm^{-1} is a characteristic of the C=O stretching of COOH, and the peak at 1,255 cm^{-1} can be attributed to the C-O stretching coupled with O-H in-plane bending. The band at 1,098 cm^{-1} is attributed to the C-O stretching. The absorbance band at 804

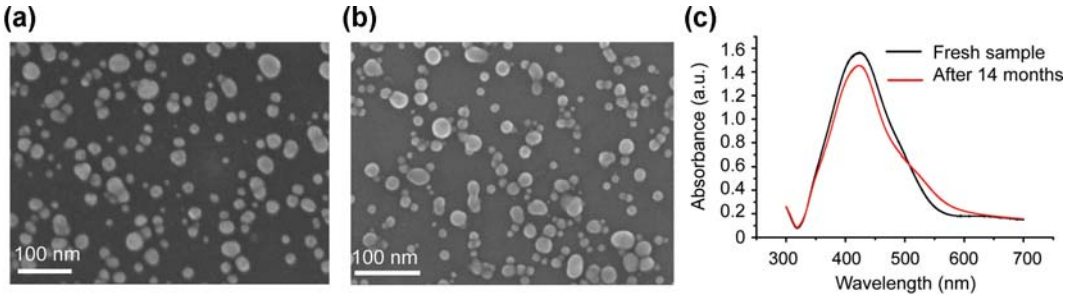

Fig. 2. (a), (b) FE-SEM image of dispersed AgNPs: (a) Freshly prepared AgNPs and (b) AgNPs after 14 months of storage in dark ambient environment. (c) UV-Vis spectra of as-synthesized AgNP solution and AgNP solution after 14 months of storage.

cm^{-1} can be attributed to the $-CH_2$ twisting and C-COOH stretching. It is noteworthy that the FTIR results agree well with previously reported findings [35], thereby confirming that the surface of the AgNPs is capped with PAA.

Additional evidence of PAA capping was obtained via elemental analysis of the synthesized AgNPs by energy-dispersive X-ray spectroscopy (EDS), whose results are shown in Fig. S2 (supplementary file). The EDS results reveal that the nanoparticles contained Ag, C, and O chemical elements. A sharp peak was observed at 3 keV because of the SPR of the nanoparticles, which is a characteristic of metallic silver [10]. Other small peaks at 0.1-0.7 keV were the characteristic peaks of the capping agent, PAA. The percentages of Ag, C, and O in the prepared AgNPs@PAA were 54.18, 14.53, and 31.28%, respectively. Hence, it can be concluded that the nanoparticles have an Ag core and a PAA layer capping the surface of this core. Our results agree well with those reported by other researchers [35,36].

The stability of the prepared AgNPs@PAA was monitored by SEM and UV-Vis spectroscopy, and the results are shown in Fig. 2. This figure depicts a comparison between freshly prepared AgNPs@PAA and AgNPs@PAA after 14 months of storage in a dark ambient environment. Figs. 2(a) and 2(b) reveal that despite the long storage period of the synthesized AgNPs, their morphology and dispersion in solution remained unchanged. Fig. 2(c) shows the UV-Vis spectrum of the freshly prepared AgNPs@PAA in comparison to that of AgNPs@PAA after 14 months of storage. A slight change in the absorbance is observed. As stated earlier, the sample was diluted 800 times before UV-Vis measurements. Fig. 2 demonstrates that the prepared AgNPs@PAA have good stability in a colloidal phase after 14 months.

2. Catalytic Performance

The catalytic performance of the as-prepared AgNPs@PAA catalyst was studied in terms of reduction of organic pollutants, such as *p*NP and MB to *p*-amino phenol (*p*AP) and leuco-methylene blue (LMB), respectively, using $NaBH_4$ as a reducing agent. The catalytic behavior was evaluated by UV-Vis spectroscopy at different time points and catalyst doses. The concentration of the reducing agent was kept much higher than those of *p*NP and MB to ensure that the $NaBH_4$ concentration remained constant throughout the reduction process. According to this stipulation, the catalytic reduction reaction can be considered as a pseudo-first-order reaction [37,38]. Hence, the reaction rate constant (k_{app}) for the reduction of *p*NP and MB can be determined using the following equation:

$$\ln\left(\frac{C_t}{C_o}\right) = -k_{app}t, \quad (1)$$

where C_o and C_t denote the initial concentration of the pollutant (*p*NP or MB) and the concentration at a certain time t, respectively. According to the Beer-Lambert law, the C_t/C_o ratio can be obtained from the corresponding absorbance ratio, A_t/A_o. Consequently, Eq. (1) can be redefined as follows:

$$\ln\left(\frac{C_t}{C_o}\right) = \ln\left(\frac{A_t}{A_o}\right) = -k_{app}t \quad (2)$$

According to Eq. (2), k_{app} corresponds to the slope of the linear relationship between t and C_t/C_o.

2-1. Catalytic Reduction of MB

The catalytic performance of the as-prepared AgNPS@PAA catalyst was examined by studying the influence of the catalyst dose in the reduction of the MB dye under a high concentration of $NaBH_4$ to ensure a pseudo-first-order reaction. In the absence of the AgNPs@PAA catalyst, the maximum absorption peak intensity of MB at λ=664 nm decreased slightly with time, without an obvious change in the solution color even after more than 1 h. Under the same conditions, the addition of the AgNPs@PAA catalyst to the reaction mixture resulted in a gradual decrease in the peak intensity of MB at λ=664 nm with time, indicating the reduction of MB to LMB. The peak intensity continued to decrease gradually, indicating a decrease in the MB concentration. This occurred until complete reduction of the MB dye was accomplished in 17 and 4.5 min for AgNPs@PAA doses of 5 and 10 μL, respectively (0.152 mg/mL, as shown in Figs. 3(a) and 3(b), respectively).

The effect of the catalyst dose on the reaction kinetics was assessed by varying the dose in the presence of excess $NaBH_4$. The reduction rate of MB was found to increase with an increase in the amount of AgNPs@PAA added to the reaction mixture. The kinetic rate was found to follow a pseudo-first-order reaction as outlined in Fig. 3(c), where k_{app} was found to increase with an increase in the amount of added catalyst. The k_{app} values for the reduction of MB to LMB under the investigated conditions were 0.199 and 0.756 min^{-1} for AgNPs@PAA doses of 5 and 10 μL, respectively (Table 2).

To compare the catalytic efficiency of the synthesized AgNPs@PAA in the reduction of MB with previously reported values, the obtained rate constant for the reduction reaction was normalized

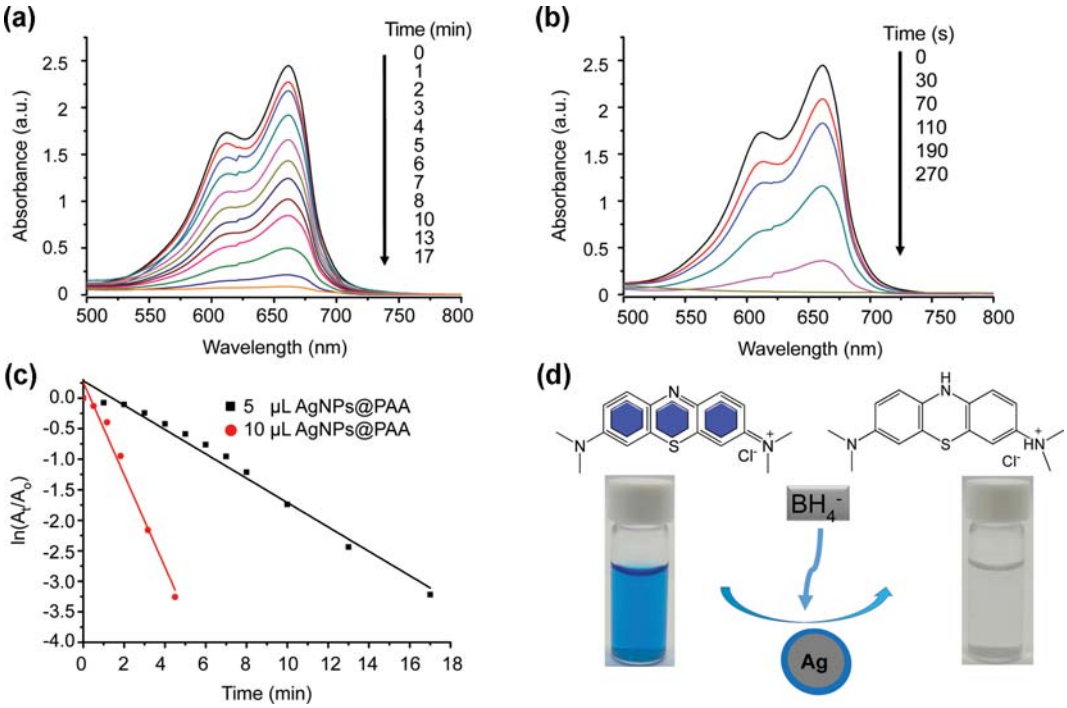

Fig. 3. (a), (b) Typical absorption spectra for catalyzed reduction of MB in the presence of $NaBH_4$ for different amounts of AgNPs@PAA: (a) 5 μL and (b) 10 μL. (c) Plot of $\ln(A_t/A_o)$ versus time for reduction of MB dye to LMB. (d) Scheme of reduction of MB to LMB in the presence of AgNPs@PAA.

Table 2. Comparison of rate constants obtained in present study with previously reported values

Catalyst structure	Pollutant	Final amount of catalyst (mg/mL)	Rate constant K_{app} (min^{-1})	Normalized rate constant K_{int} ($L/min^{-1}\cdot g^{-1}$)	Reference
AgNPs@PAA	MB	2.54×10^{-4}	0.199	783.5	This study
AgNPs@PAA	MB	5.07×10^{-4}	0.756	1566.9	This study
Fe_3O_4@PDA-Ag	MB	0.48	0.430	0.9	[40]
Au@PPy/Fe_3O_4	MB	0.57	0.266	0.47	[41]
D-graphene/Ag(40%)	MB	0.049	0.2523	5.1	[42]
CF-AuNPs-2.87	MB	0.2	8.1×10^{-5}	4.02×10^{-4}	[43]
Au@TA-GH	MB	0.077	0.31	4.03	[44]
Ni@C(N)	MB	0.08	1.93	24.12	[45]
AgNPs@PAA	*p*NP	1.014×10^{-4}	0.089	881.2	This study
AgNPs@PAA	*p*NP	2.027×10^{-4}	0.461	2270.1	This study
Ag-p(NIPAAm-HEMA-AAc)	*p*NP	0.04	0.873	21.83	[39]
Ag/Triton X-705/TMB	*p*NP	2.4	0.312	0.13	[46]
Ag-CAHB	*p*NP	2	0.894	0.45	[47]
Pt@AgNPs	*p*NP	0.01667	0.355	21.4	[48]
GO@NH_2-AuNCs	*p*NP	0.004	2.136	534	[49]
GOAFe_3O_4AAuNPs	*p*NP	0.0066	1.93	289.7	[50]
Co-$CoFe_2O_4$ nanobrushes	*p*NP	0.1	2.75	27.4	[51]
AgNPs/MWCNTs@S. L.	pNP	0.06	1.152	19.2	[52]

(K_{int}) according to the following equation [39]:

$$K_{int} = \frac{K_{app}}{m/\text{Volume of reaction mixture}}, \quad (3)$$

where m is the final amount of catalyst added in the catalytic reduction reaction. Table 2 lists the calculated K_{int} values for our catalyst in comparison to those reported previously under similar conditions [40-45]. The data summarized in Table 2 show that K_{int} for the catalytic reduction of MB using 10 μL (0.152 mg/mL) of the highly stable AgNPs@PAA is higher than that using a dose of 5 μL under the same conditions. From the K_{int} values in Table 2, it is determined that the synthesized AgNPs@PAA catalyst has superior catalytic activity when compared to other previously reported catalysts for MB reduction.

MB and BH_3^- are adsorbed onto the surface of the AgNPs@PAA catalyst, which acts as a transmitter of electrons from the electron donor BH_4^- to the electron acceptor MB. Hence, the reduction reaction of MB is catalyzed as outlined in Fig. 3(d). The increase in the reduction rate with an increase in the amount of the AgNPs@PAA catalyst, as revealed in Table 2, is due to the increase in the number of active sites on the AgNPs@PAA surface. The high catalytic activity of the prepared AgNPs@PAA is a result of the uniform and small particle size of the AgNPs. Consequently, the synthesized catalyst provides a high surface area-to-volume ratio for high adsorption of MB with a great electronic transport capability.

2-2. Catalytic Reduction of *p*NP

The catalytic activity of the AgNPs@PAA catalyst for the reduction of the *p*NP pollutant to *p*AP using a high concentration of $NaBH_4$ as a reducing agent was also evaluated. It is known that *p*NP has a strong absorption band at λ=317 nm. Moreover, upon the addition of a reducing agent, the solution color changes from pale yellow to bright yellow along with a peak shift to λ=400 nm because of the conversion of *p*-nitrophenol into *p*-nitrophenolate. In the absence of the AgNPs@PAA catalyst, the absorption peak at λ=400 nm shifted very slightly over a 60-min period, without any obvious change in the solution color. In the presence of the AgNPs@PAA catalyst, the intensity of the absorption peak at λ=400 nm decreased gradually with time, indicating the reduction of *p*NP with the formation of a new band at λ=300 nm. The newly formed band is associated with the formation of *p*AP, whose concentration increases with time in the case of addition of 2 and 4 μL of AgNPs@PAA (0.152 mg/mL), as depicted in Figs. 4(a) and 4(b), respectively.

The effect of the amount of catalyst on the reaction kinetics was assessed by varying the catalyst dose in the presence of excess $NaBH_4$. The reduction rate of *p*NP increased with an increase in the amount of added AgNPS@PAA catalyst. The reduction reaction was predicted to follow a pseudo-first-order reaction because of the use of a high concentration of $NaBH_4$. According to Eq. (2), the kinetic rate was found to follow a pseudo-first-order reaction, as outlined in Fig. 4(c). The k_{app} values for the reduction of *p*NP to *p*AP were 0.089 and 0.461 min^{-1} for AgNPs@PAA doses of 2 and 4 μL, respectively.

The K_{int} value for the catalytic reduction of *p*NP was calculated according to Eq. (3), and the calculated data are listed in Table 2. The calculation results show that K_{int}, for the catalytic reduction of *p*NP, increased with an increase in the amount of added catalyst. This indicates that the use of 4 μL of the AgNPs@PAA catalyst (0.152 mg/mL) resulted in better catalytic activity than the use of 2 μL of the catalyst. The calculated K_{int} values for our catalyst in comparison to those reported in the literature [39,46-50] are summarized in Table 2.

Both *p*NP and BH_4^- were adsorbed onto the surface of AgNPs@PAA; this facilitated the transportation of electrons from BH_4^- to *p*NP via their respective active sites, as outlined in Fig. 4(d). The reduction rate increased with an increase in the amount of added AgNPs@PAA catalyst, as revealed in Table 2. This behavior was due to the increase in the number of active sites on the AgNPs@PAA surface.

The synthesized AgNPs@PAA catalyst utilized for the *p*NP reduction was recyclable. After completion of the reduction process, the catalyst was separated by centrifugation. The catalytic efficiency was evaluated after repeated use for up to seven cycles, and it was determined to be stable with a conversion of approximately 99.7% (Fig. 4(e)). This significant recyclability may be a result of the high

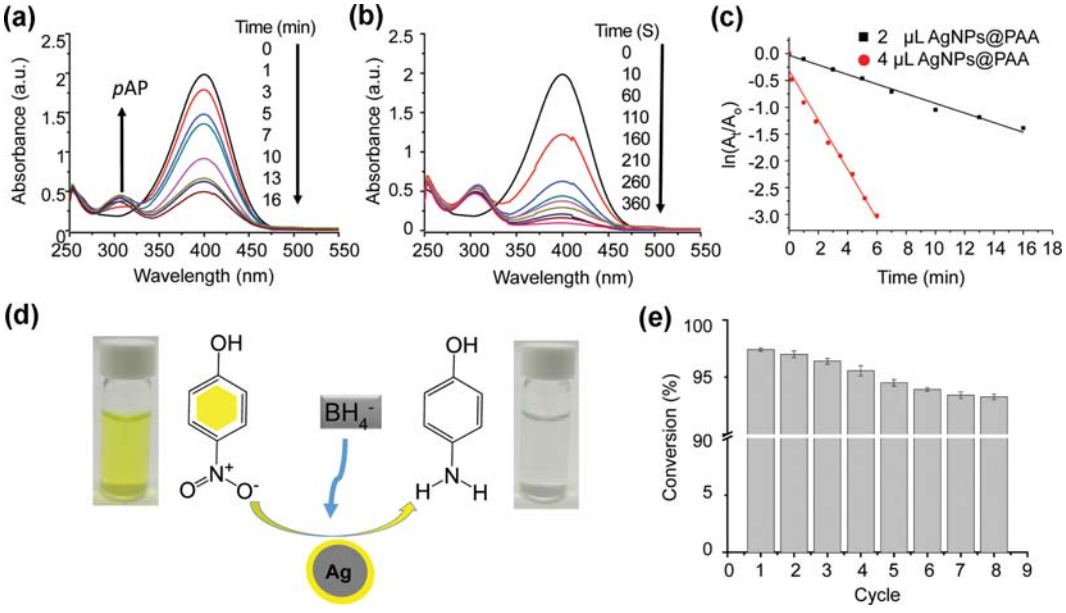

Fig. 4. (a), (b) Typical absorption spectra for catalyzed reduction of *p*NP in the presence of $NaBH_4$ for different amounts of AgNPs@PAA: (a) 2 μL and (b) 4 μL. (c) Plot of $\ln(A_t/A_o)$ versus time for reduction of *p*NP dye to *p*AP. (d) Scheme of reduction of *p*NP to *p*AP in the presence of AgNPs@PAA catalyst. (e) Catalytic efficiency of synthesized AgNPs after repeated use (error bars represent the standard deviation of four replicates).

stability of the AgNPs in aqueous solution, which, in turn, was believed to be caused by the carboxylate anions of PAA that acted as a stabilizing agent. The supernatant of the centrifuged solution was analyzed via ICP-MS to determine whether the nanoparticles were leached out. Further, a quantitative analysis of the released silver was performed after seven cycles of use and no significant amount of silver was detected. Therefore, it can be concluded that our synthesized AgNPs@PAA catalyst remained stable even after seven cycles of use.

CONCLUSION

A benign, one-pot, low-cost, and environmentally friendly process based on a wet chemistry technique was developed for synthesizing AgNPs. In particular, a highly concentrated, stable colloid of AgNPs with a high reaction efficiency (92.4%) was synthesized using a wet-chemical strategy. The technique employed in this study is advantageous over those used in other studies in that it yields highly concentrated nanoparticles with a narrow size distribution (14.83±5.96 nm). The coating of AgNPs with PAA was found to enhance their colloidal stability (that is, they were stable even after more than 14 months), and these coated AgNPs showed improved catalytic performance in the reduction of *p*NP and MB to *p*AP and LMB, respectively, in the presence of $NaBH_4$. The prepared AgNPs@PAA showed high catalytic activity with good recyclability. It can be concluded that the nanoparticles synthesized by this simple process have potential for use in diverse industrial applications; for example, they can be used as antimicrobial agents; for localized SPR; and in sensors, catalysts, medicine, electronics, and even flexible circuits.

ACKNOWLEDGEMENT

This work was supported by the National Research Foundation of Korea (NRF) grant (R201901411).

COMPETING INTEREST

There are no competing interests to declare.

SUPPORTING INFORMATION

Additional information as noted in the text. This information is available via the Internet at http://www.springer.com/chemistry/journal/11814.

REFERENCES

1. K. M. Mayer and J. H. Hafner, *Chem. Rev.*, **111**, 3828 (2011).
2. R. Jin, *Nanoscale*, **7**, 1549 (2015).
3. Y. Li, Y. Wu and B. S. Ong, *J. Am. Chem. Soc.*, **127**, 3266 (2005).
4. W. Shen, X. Zhang, Q. Huang, Q. Xu and W. Song, *Nanoscale*, **6**, 1622 (2014).
5. M. Potara, A. M. Gabudean and S. Astilean, *J. Mater. Chem.*, **21**, 3625 (2011).
6. M. Baccarin, B. C. Janegitz, R. Berte, F. C. Vicentini, C. E. Banks, O. Fatibello and V. Zucolotto, *Mat. Sci. Eng. C-Mater.*, **58**, 97 (2016).
7. X. Chen and H. J. Schluesener, *Toxicol. Lett.*, **176**, 1 (2008).
8. W. C. Zhang, Y. Sun and L. Zhang, *Ind. Eng. Chem. Res.*, **54**, 6480 (2015).
9. M. Rai, A. Yadav and A. Gade, *Biotechnol. Adv.*, **27**, 76 (2009).
10. S. Agnihotri, S. Mukherji and S. J. R. A. Mukherji, *Rsc Adv.*, **4**, 3974 (2014).
11. H. S. Toh, K. Jurkschat and R. G. Compton, *Chemistry*, **21**, 2998 (2015).
12. S. Mandal, A. Gole, N. Lala, R. Gonnade, V. Ganvir and M. Sastry, *Langmuir*, **17**, 6262 (2001).
13. Y. Lu, G. L. Liu and L. P. Lee, *Nano Lett.*, **5**, 5 (2005).
14. Y. Wang, J. F. Wong, X. Teng, X. Z. Lin and H. Yang, *Nano Letters*, **3**, 1555 (2003).
15. W. Y. William, C. Emmanuel, M. S. Christie, D. Rebekah and L. C. Vicki, *Nanotechnology*, **17**, 4483 (2006).
16. W. W. a. B. Gu, Concentrated Dispersions Theory, Experiment, and Applications, American Chemical Society, Wasgington DC (2004).
17. H. S. Devi, N. R. Singh and T. D. Singh, *Arab. J. Sci. Eng.*, **41**, 2249 (2016).
18. Y. S. Liu, S. M. Chen, L. Zhong and G. Z. Wu, *Radiat. Phys. Chem.*, **78**, 251 (2009).
19. S. Iravani, H. Korbekandi, S. V. Mirmohammadi and B. Zolfaghari, *Res. Pharm. Sci.*, **9**, 385 (2014).
20. Q. J. Huang, W. F. Shen, Q. S. Xu, R. Q. Tan and W. J. Song, *Mater. Chem. Phys.*, **147**, 550 (2014).
21. S. Magdassi, M. Grouchko, O. Berezin and A. Kamyshny, *Acs Nano*, **4**, 1943 (2010).
22. Y. S. Shon and E. Cutler, *Langmuir*, **20**, 6626 (2004).
23. I. Sondi, D. V. Goia and E. Matijevic, *J. Colloid Interface Sci.*, **260**, 75 (2003).
24. H. Aldewachi, T. Chalati, M. N. Woodroofe, N. Bricklebank, B. Sharrack and P. Gardiner, *Nanoscale*, **10**, 18 (2018).
25. K. Toisawa, Y. Hayashi and H. Takizawa, *Mater. Trans.*, **51**, 1764 (2010).
26. A. Mari, P. Imperatori, G. Marchegiani, L. Pilloni, A. Mezzi, S. Kaciulis, C. Cannas, C. Meneghini, S. Mobilio and L. Suber, *Langmuir*, **26**, 15561 (2010).
27. J. P. Yang, H. J. Yin, J. J. Jia and Y. Wei, *Langmuir*, **27**, 5047 (2011).
28. R. M. Molnar, M. Bodnar, J. F. Hartmann and B. Janos, *Colloid Polym. Sci.*, **287**, 739 (2009).
29. J. Ge, Y. Hu, M. Biasini, C. Dong, J. Guo, W. P. Beyermann and Y. Yin, *Chemistry*, **13**, 7153 (2007).
30. Y. X. Hu, J. P. Ge, D. Lim, T. R. Zhang and Y. D. Yin, *J. Solid State Chem.*, **181**, 1524 (2008).
31. J. Ge, Y. Hu, M. Biasini, W. P. Beyermann and Y. Yin, *Angew Chem. Int. Ed. Engl.*, **46**, 4342 (2007).
32. C. Kastner and A. F. Thunemann, *Langmuir*, **32**, 7383 (2016).
33. T. K. Sau, A. Pal and T. Pal, *J. Phys. Chem. B*, **105**, 9266 (2001).
34. Z. M. Zheng, Q. L. Huang, H. Guan and S. Y. Liu, *Rsc Adv.*, **5**, 69790 (2015).
35. J. Billingham, C. Breen and J. Yarwood, *Vib. Spectrosc.*, **14**, 19 (1997).
36. J. Dong, Y. Ozaki and K. Nakashima, *Macromolecules*, **30**, 1111 (1997).
37. X. Zhao, Q. D. An, Z. Y. Xiao, S. R. Zhai and Z. Shi, *Chinese J. Catal.*, **39**, 1842 (2018).

38. H. Mao, C. G. Ji, M. H. Liu, Z. Q. Cao, D. Y. Sun, Z. Q. Xing, X. Chen, Y. Zhang and X. M. Song, *Appl. Surf. Sci.*, **434**, 522 (2018).
39. R. Begum, Z. H. Farooqi, Z. Butt, Q. Wu, W. Wu and A. Irfan, *J. Environ. Sci. (China)*, **72**, 43 (2018).
40. Y. Xie, B. Yan, H. Xu, J. Chen, Q. Liu, Y. Deng and H. Zeng, *ACS Appl. Mater. Inter.*, **6**, 8845 (2014).
41. T. Yao, T. Cui, H. Wang, L. Xu, F. Cui and J. Wu, *Nanoscale*, **6**, 7666 (2014).
42. P. K. Sahoo, N. Kumar, S. Thiyagarajan, D. Thakur and H. S. Panda, *Acs Sustain. Chem. Eng.*, **6**, 7475 (2018).
43. M. T. Islam, N. Dominguez, M. A. Ahsan, H. Dominguez-Cisneros, P. Zuniga, P. J. J. Alvarez and J. C. Noveron, *J. Environ. Chem. Eng.*, **5**, 4185 (2017).
44. J. Luo, N. Zhang, J. Lai, R. Liu and X. Liu, *J. Hazard Mater.*, **300**, 615 (2015).
45. G. M. Shi, S. T. Li, F. N. Shi, X. F. Shi, S. H. Lv and X. B. Cheng, *J. Colloids Surf., A*, **555**, 170 (2018).
46. M. Bano, D. Ahirwar, M. Thomas, G. A. Naikoo, M. U. D. Sheikh and F. Khan, *New J. Chem.*, **40**, 6787 (2016).
47. C. Gao, Q. D. An, Z. Y. Xiao, S. R. Zhai, B. Zhai and Z. Shi, *New J. Chem.*, **41**, 13327 (2017).
48. Z. S. Lv, X. Y. Zhu, H. B. Meng, J. J. Feng and A. J. Wang, *J. Colloid Interface Sci.*, **538**, 349 (2018).
49. Y. Y. Ju, X. Li, J. Feng, Y. H. Ma, J. Hu and X. G. Chen, *Appl. Surf. Sci.*, **316**, 132 (2014).
50. J. Hu, Y.-l. Dong, X.-j. Chen, H.-j. Zhang, J.-m. Zheng, Q. Wang and X.-g. Chen, *Chem. Eng. J.*, **236**, 1 (2014).
51. Y. Zhang, H. Fang, Y. Zhang, M. Wen, D. Wu and Q. Wu, *J. Colloid Interface Sci.*, **535**, 499 (2019).
52. H. Veisi, S. Kazemi, P. Mohammadi, P. Safarimehr and S. Hemmati, *Polyhedron*, **157**, 232 (2019).